A study of the uptake of hydrogen in pipeline steels using accelerated laboratory methodologies

Patrick Kambilinya[1*], *Tresor* Mapoli[1*], *Eric* Peter[1*], *Joseph* Moema[2], *Charles* Siyasiya[1], *and Roelf* Mostert[1]

[1]Department of Materials Science and Metallurgical Engineering, University of Pretoria, South Africa,
[2]Advanced Materials Division, physical Metallurgy group, MINTEK, South Africa.

Abstract. The study investigates hydrogen uptake in two pipeline steels using accelerated laboratory methods. Thermal desorption mass spectrometry (TDMS) was used for diffusible hydrogen content and hydrogen trap analysis. The optimal electrolyte for electrochemical charging was found to be 1.0 N H_2SO_4 + 3% NH_4SCN. TDMS confirmed hydrogen uptake, with the highest levels observed for the time between 36 and 48 hours of charging. The study of hydrogen permeability compared the steels' susceptibility to hydrogen uptake, with the steel A showing a greater capacity for hydrogen uptake than steel B.

1 Introduction

The world is progressing and transitioning into a sustainable and greener economy by aiming at reducing carbon emissions. Globally, green hydrogen is highly sought after as an essential component in energy transition plans as it is a low-emission energy carrier ideally suited for sectors that are hard to decarbonise, such as transportation, heating and power production [1]. South Africa is pursuing the hydrogen economy as a strategic development opportunity to emerge as a major producer of green hydrogen [2]. Safe storage and transportation of hydrogen are vital for the growth of a hydrogen economy, and existing pipelines used in the oil and natural gas sectors are attractive modes of hydrogen transportation, but corrosion and gaseous hydrogen embrittlement (GHE) are associated risks [3].

HE in steel causes loss of ductility and fracture, jeopardising the integrity and safety of the pipelines. HE follows the dissociation of molecular hydrogen and diffusion of atomic hydrogen into the steel microstructure where it accumulates and interacts with trap sites such as vacancies, grain boundaries, dislocations and interfaces between matrix and particles, including carbides [4]. Pressurised molecular hydrogen is generally harmless to metals, but it is known to dissociate into atomic hydrogen, which causes the HE [5]. The severity of HE is influenced by factors such as the total absorbed hydrogen concentration, the nature of trapping sites, applied stress and microstructural features, making it a complex problem to

*pkambilinya2@gmail.com, *tresormapoli@gmail.com, *ericp692@gmail.com

address. The amount of diffusible H in a metal directly correlates to its HE sensitivity index, which is the measure of how much a particular metal is susceptible to HE [6]. It also correlates to the nature of H trapping sites available in the steel's microstructure which are classified as either reversible or irreversible traps. Irreversible traps are those microstructural sites where an H atom has an infinite residence relative to the timescale for a permeation test due to the binding energy relative to the migration energy for diffusion [7][8][9]. Reversible traps are microstructural sites where an H atom has a shorter residence and lower binding energy. There are many techniques to study and evaluate hydrogen uptake, including accelerated techniques such as thermal desorption mass spectrometry (TDMS), electrochemical permeation tests and gaseous exposure. This paper focuses on testing for diffusible H or H–uptake using the aforementioned accelerated laboratory techniques.

2 Experimental procedure and materials

2.1 Materials

In this study, two different grades (steel A and B) of hot-rolled high strength low alloy (HSLA) strip steel with a thickness of 4 mm were investigated. These grades are typically used in the manufacture of linepipe steel used in the pipeline industry. The chemical composition of the two 4 mm thick plate steel sections was determined by mass spectrometry as shown in Table 1.

Table 1. Chemical composition of the studied steels in weight%.

Steel	C	Mn	P	S	Si	Cu	Ni	Cr	Nb	Ti	Al
A	0.044	0.998	0.012	0.002	0.02	0.01	0.02	0.003	0.018	0.018	0.028
B	0.041	1.76	0.015	0.002	0.1	0.02	0.02	0.269	0.066	0.101	0.037

Standard metallographic sample preparation and etching with Nital 2% Nital solution was performed. Metallographic analysis of the steels was done using an Olympus optical microscope and revealed a heterogeneous and anisotropic distribution of ferrite and pearlite in both steels as shown in Fig. ***3***. Before the electrolytic charging, hydrogen permeation test and gaseous exposure experiments, the specimens were polished up to 1200 grit size using SiC abrasive paper to remove the oxide layer and machining defects on the steel surface. The prepared samples were then cleaned with acetone and dried with compressed air.

2.2 Methods

To simulate pipeline hydrogen permeation, atomic hydrogen was introduced in the steels through two electrochemical techniques: hydrogen cathodic charging and a double cell hydrogen permeation technique, as well as a pressurised gaseous hydrogen (H_2) exposure technique.

2.2.1 Electrochemical techniques

Before the electrochemical charging (which include the cathodic and H double cell permeation technique), polarisation scans were performed to determine the appropriate electrolyte solution and charging conditions using an Autolab PGSTAT302N potentiostat. The electrolyte was prepared using the H_2SO_4 concentrated at 98.08% and NH_4SCN as a

hydrogen recombination inhibitor, and all dissolved in de-ionised water. Ammonium salts such as ammonium chloride, ammonium sulphate, ammonium nitrate and ammonium carbonate are used as inhibitors because they are known to possess relatively good ionic conductivity and good thermal stability. NH_4SCN has been reported to have a lower lattice energy of 605 $kJmol^{-1}$; thus, when NH_4SCN is dissolved into a solvent such as water or acetic acid, it easily dissociates into the cation and anion species [10]. Electrolytes of 1.0N H_2SO_4 plus varying percentages of the hydrogen recombination inhibitor (NH_4SCN) were used. Before any experiment, the electrolyte was purged for 30 minutes using nitrogen gas. The cathodic region of the steels was determined by assessing the corrosion behaviour of the steels in the studied environments by cathodically polarising the samples from the open-circuit potential (OCP). Every sample was first immersed for 55 minutes to achieve a stable OCP current before running the potentiodynamic polarization scan. The applied potential range was from -1.5 to 0.4 V, using a scan rate of 1.0 mVs^{-1} at room temperature (30°C) with no stirring. Therefore, the preferred electrolyte for both steels was determined to be 1.0N H_2SO_4 + 3% NH_4SCN as generally, higher current densities were detected through this media (Fig. ***4*** a–c). This was confirmed later through TDMS results in Fig. ***6*** (c) and (d). From the polarisation scans obtained, the applied potential of -1 V was determined. A conventional three-electrode set-up was used with the steel specimens as the working electrode (WE). A platinum sheet electrode served as a counter electrode (CE), and a saturated Ag/AgCl was the reference electrode (RE). The potentiodynamic analysis was carried out using an AUTOLAB PGSTAT302N potentiostat, and data were analysed using the NOVA version 1.8 software provided by AUTOLAB. The cathodic charging was then done using a fixed potential of -1 V and varying times of 24, 36, 48 and 72 hours successively.

The Devanathan–Stachurski (D-S) double cell setup according to ASTM G148 [11] was used for the hydrogen permeation experiments using a Metrohm DropSens µStat-i MultiX multichannel potentiostat. The tests were conducted on a 40 mm square steel sample with a thickness of 1 mm. The sample was inserted in between the charging (cathodic) and the oxidation (anodic) cell as illustrated in the Fig. ***1*** (working electrode).

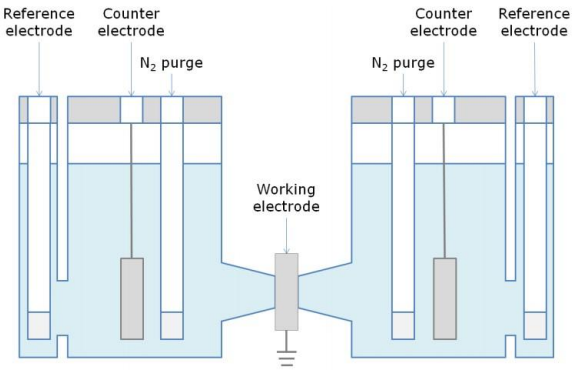

Fig. 1. Schematic representation of the Devanathan–Stachurski double cell setup [12].

The electrolytes that were contained in the oxidation and charging cell were 0.1 mol/l NaOH and 1.0N H_2SO_4 in combination with 3% NH_4SCN, respectively. Prior to the permeation test, all the electrolytes were subjected to vigorous purging with nitrogen gas for 30 minutes to deaerate the solutions. The samples were preheated in a muffle furnace at 80 ºC overnight (16 hours) before the experiment to remove any traces of mobile hydrogen already present in the material. Before the first charging cycle, amperometric detection was done in the oxidation cell by applying +300 mV. The decay current in the oxidation cell was monitored until it stabilised as close to zero µA as possible. Two charging cycles with an

intermediate discharge were performed to distinguish the effects of irreversible and reversible trapping on hydrogen transport. The intermediate discharging step involved a complete deactivation of the charging cell after the attainment of a steady state followed by decanting of the solution. A decay of the permeation current in the oxidation cell, indicative of diffusing out of all mobile hydrogen, was then monitored until it stabilised as low as possible before the second charging cycle was activated. The charging transients were performed at a current density of -1 mA/cm^2, while the oxidation cell was maintained at a potential of +300 mV (SCE) in accordance with ASTM G148 [11]. The effective diffusion coefficients (D_{eff}), the subsurface hydrogen concentration on the charging side (C_0) and the time to achieve steady state (t_{lag}) were determined by the time lag method based on Fick's Laws and were automatically calculated by the H_2 permeation module implemented in the DropView 8400M software using the following equations [11]:

$$D_{eff} = \frac{L^2}{6t_{lag}} \quad (1)$$

$$J_{SS} = \frac{D_{eff}C_0}{L} \quad (2)$$

Where L and J_{ss} are the sample thickness and atomic hydrogen permeation flux at steady state, respectively.

2.2.2 Gaseous exposure technique

Hydrogen uptake in steels is strongly influenced by temperature and pressure as described by the ideal gas law and can therefore occur across a wide range of conditions. Temperature plays a crucial role by governing the H solubility, diffusivity and surface reaction effects with the material [13]. Gaseous charging tests are widely used to characterise these effects, whereby steel samples are subjected to high–pressure H environment at elevated temperatures. Experimental conditions typically range from pressures within 100–1000 bar and temperatures 20–600°C [14][15], although in service applications such as natural gas pipelines, operating temperatures are generally lower, between 20–60°C. In this study, a gaseous hydrogen (H_2) exposure technique was adopted using an autoclave (Parr Model 4670–1G movable head pressure vessel with heater and 4838 controller). The gaseous exposure technique investigated H-permeation at a temperature of 260°C and pressure of 100 bar H_2 pressure for a duration of 7 days.

2.2.3 Thermal desorption mass spectrometry technique

Before the charged samples were taken for TDMS, they were immediately immersed in liquid nitrogen to minimise H diffusing out of the sample thereby preserving the H content. To determine the H content in both steels (charged vs uncharged), the TDMS technique was performed using the Bruker Hydrogen Analyser-G4 Phoenix DH. The test procedure involves heating of samples in a quartz extraction tube with an infrared furnace. Before the thermal conductivity of the gas is examined, an inert carrier gas (nitrogen) is pushed through the quartz tube, which then goes through a number of molecular sieves to eliminate moisture (H_2O) and carbon dioxide. Because more carrier gas is injected into the furnace quartz tube than is pushed through the system, the system is open. By producing a back pressure, this isolates the system from the atmosphere. Diffusible hydrogen in the examined sample is desorbed during heating, and the carrier gas subsequently carries it to the detector. The hydrogen content is then determined as a function of the change in the thermal conductivity. For the current study, the samples were heated from room temperature to the maximum temperature of 900°C using a ramp rate of 50°C/min and soaked for 15 minutes.

3 Results and discussion

3.1 Microstructural analysis

Fig. ***3*** shows optical micrographs of the two steels in the normal, transverse and longitudinal directions (ND, TD, LD) respectively as indicated by the schematic in Fig. ***2***. The microstructures show a heterogeneous and anisotropic distribution of ferrite and pearlite in both steels.

A classic equiaxed ferrite–pearlite microstructure was observed especially in steel A, as well as clearly defined ferrite grain boundaries. A coarser ferrite grain size distribution and higher volume fraction of pearlite are observed in steel A as compared to steel B. Steel B showed a microstructure of acicular ferrite and fine, well distributed carbides. This could be attributed to the higher content of alloying elements such as Ti, Nb (grain refiners) and Mn, Cr (carbide former elements retarding austenite decomposition) in steel B than steel A [16], [17], [18].

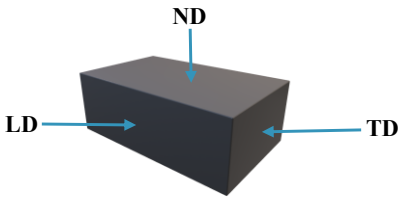

Fig. 2. Showing the steel plate's orientation directions from which samples for microstructural analysis were taken with respect to the longitudinal (hot rolling) direction.

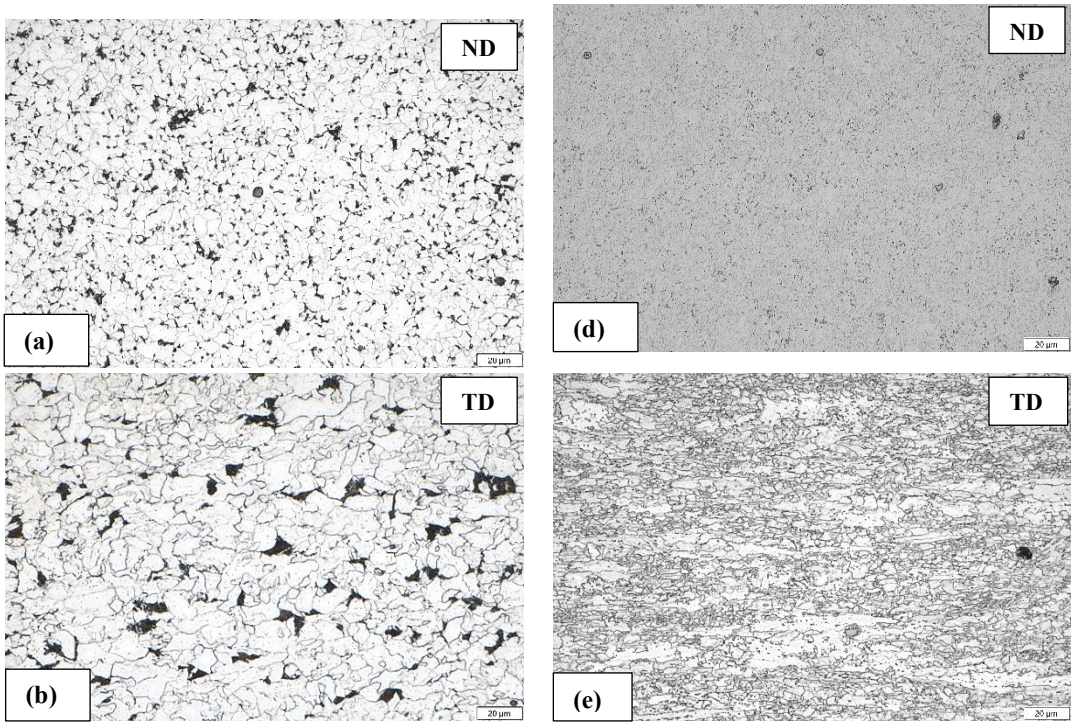

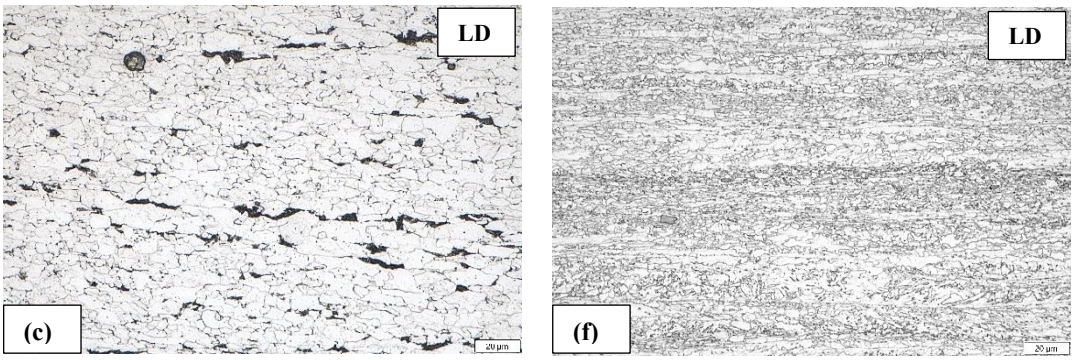

Fig. 3. Optical micrographs of (a)–(c) steel A; (d)–(f) steel B in the normal, transverse and longitudinal directions, respectively, as shown in the inserts (ND, TD, LD).

3.2 Electrochemical techniques

3.2.1 Effect of an inhibitor in electrolyte

The effect of a recombination inhibitor in the electrolyte was investigated. As a result, NH_4SCN promotes hydrogen adsorption in steel by preventing the recombination of hydrogen and hence increasing the amount of hydrogen that is adsorbed onto the steel surface and absorbed into the steel matrix [19],[20].

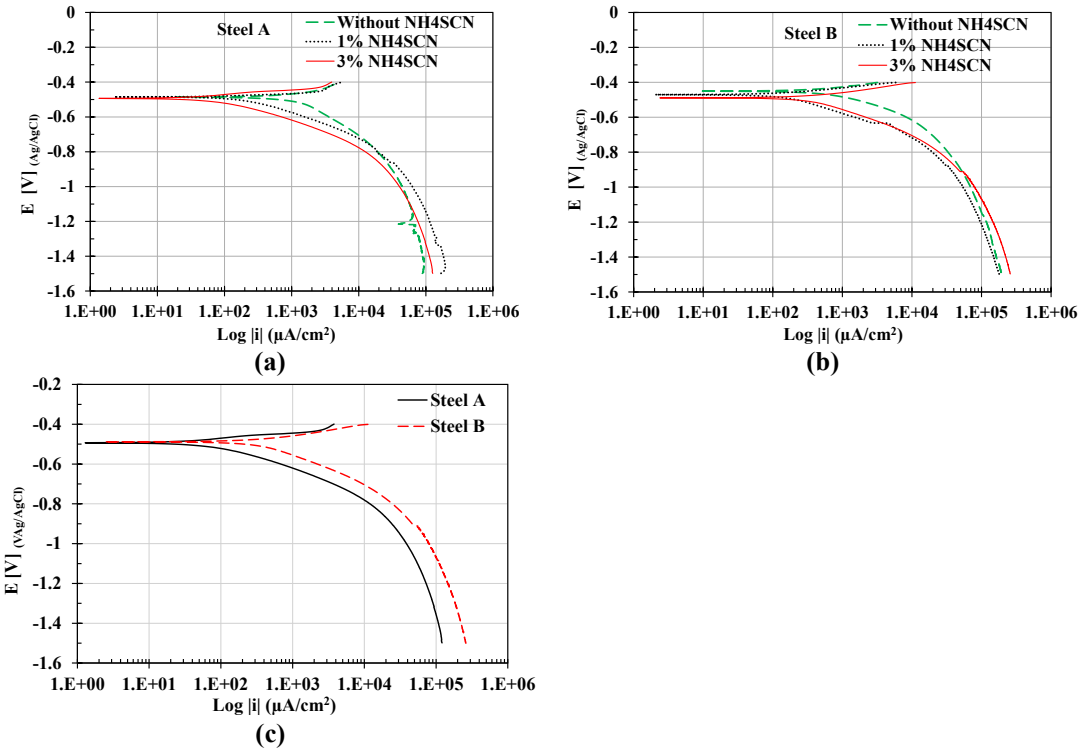

Fig. 4. (a)–(b) shows the polarization scans using 1.0N H_2SO_4 with the variation of NH_4SCN concentration for Steel A and B respectively; (c) cathodic polarization scans under 1.0N H_2SO_4 + 3% NH_4SCN.

The polarization plots in Fig. ***4*** (a–c) show that higher current densities are achieved for potentials less than -1 V as per the addition of 3% NH_4SCN solution (especially for steel B). The higher current densities translate to higher hydrogen uptake by the steel during charging. Even though the polarisation plot for steel A (Fig. ***4*** a) shows higher current densities for the 1% NH_4SCN addition, the optimal electrolyte for both steels was established with the 3% NH_4SCN addition as the higher hydrogen content was detected in the TDMS results as shown in Fig. *7*.

3.2.2 Hydrogen permeation

Fig. **5** (a) and (b) show the relevant H permeation–decay transient plots for Steel A and B obtained from the D-S double cell technique. The characteristic values that were obtained from the permeation transients of the electrochemical permeation experiments include: the D_{eff}, C_0 and t_{lag} as shown in the Table 2. According to the widely accepted theory, irreversible traps are effective during the initial transient but progressively fill as the observed hydrogen flux increases to a steady state [11][21]. Only reversible traps are thought to be involved in the second transients. In H permeation experiments, the D_{eff} during the initial transient is usually higher than in the second transient, as it is affected by the presence of trapping sites in the material. Initially, these trapping sites are mainly unoccupied which allows for faster H diffusion. In the second transient, most of the trapping sites become saturated, thereby hindering further diffusion resulting in a lower D_{eff} [11]. It can also be observed that the absorbed hydrogen content (subsurface) associated with the second transient is greater than that after the first transient, as depicted by C_0–values. It can be seen that steel A has a higher diffusivity coefficient than steel B and the t_{lag} is much faster for steel A than B as shown in Table 2. It can therefore, be deduced that steel A is more susceptible to hydrogen uptake than steel B.

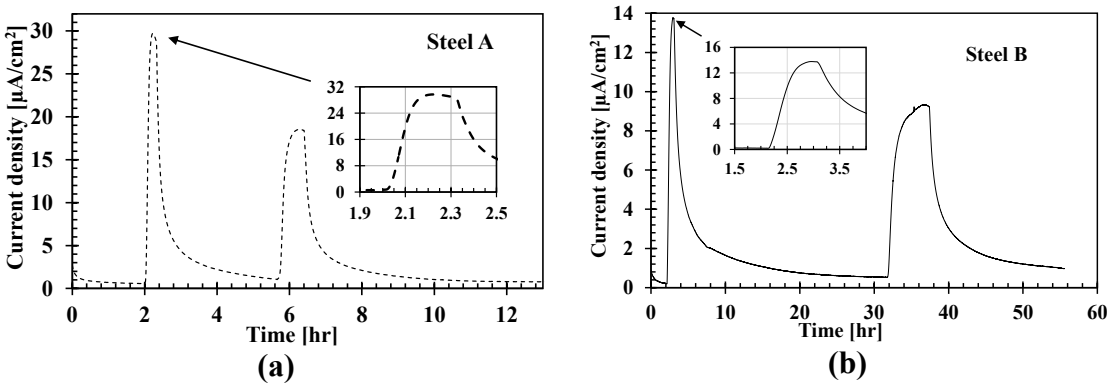

Fig. 5. (a)–(b) H permeation–decay transient plots for steel A and B, respectively.

Table 2. A comparison of the hydrogen permeation transients from Fig. *5*.

	1st transient			2nd transient		
Steel	**D_{eff} [cm^2/s]**	**C_0 [mol/m^3]**	**t_{lag} [min]**	**D_{eff} [cm^2/s]**	**C_0 [mol/m^3]**	**t_{lag} [min]**
A	3.33×10^{-6}	9.24	8.30	5.69×10^{-7}	33.60	48.80
B	1.90×10^{-6}	12.5	40.60	6.90×10^{-7}	23.40	112.30

3.3 Cathodic charging, gaseous exposure and hydrogen content detection

3.3.1 Cathodic charging

The TDMS was employed to determine the diffusible hydrogen content in charged and uncharged specimens for both steels as shown in Fig. ***6***. For the uncharged steel samples A and B, the amount of diffusible hydrogen was found to be 0.40 and 0.32 ppm, respectively. For the charging times of 24, 36, 48 and 72 hours, for steel A the amounts of diffusible hydrogen detected were 7.05, 20.87, 21.03 and 15.78 ppm, respectively. For steel B the amounts of diffusible hydrogen detected were 4.39, 8.54, 3.97 and 4.54 ppm, respectively.

TDMS results show that the optimum charging times are between 36 and 48 hours (saturation) as higher diffusible hydrogen content was detected as shown in Fig. *7*. It can be seen that lower amounts of diffusible hydrogen were detected during charging times of 24 and 72 hours. A decrease in the H content after extended charging hours (72hrs in this case) could be attributed to some factors such as formation of surface films that impede further absorption, or internal diffusible H escape mechanisms from reversible traps [22]. This normally happens at very long charging times. This can be attributed the complete filling of all reversible and/or irreversible trapping sites as discussed in section 3.2.2.

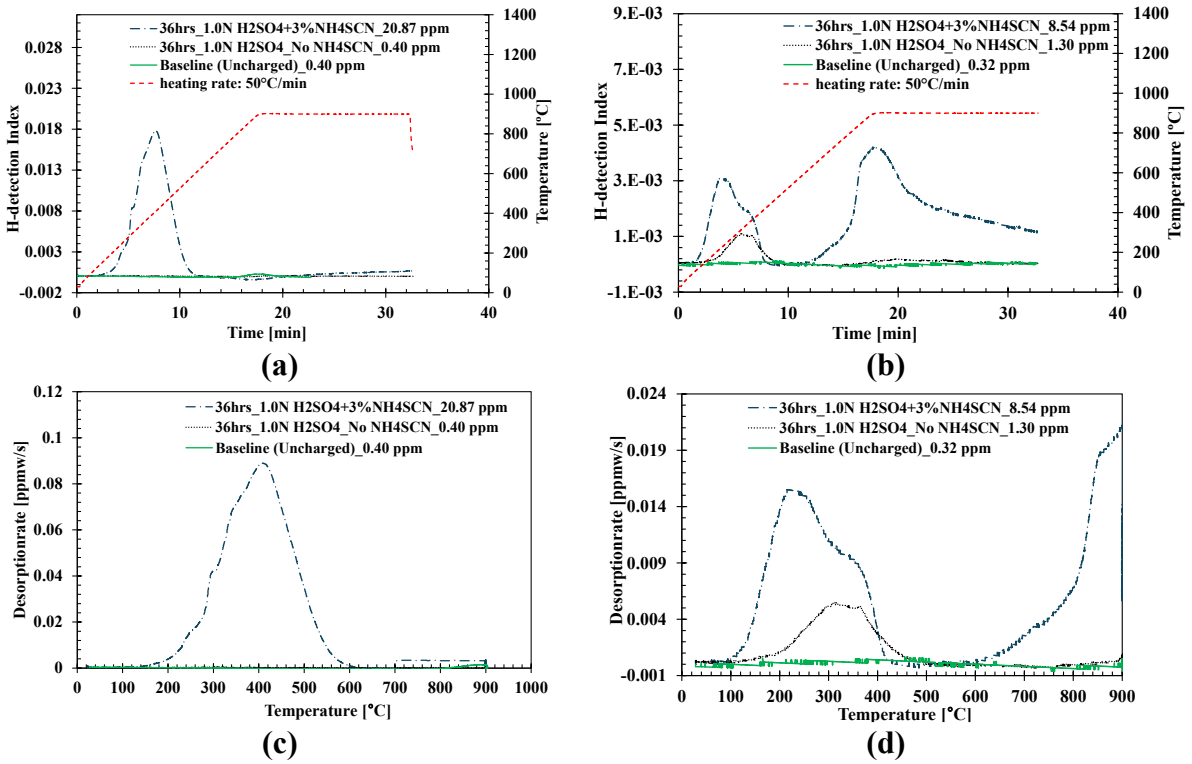

Fig. 6. (a)–(b) H detection per cycle plot for steel A and B varying NH_4SCN concentrations; (c)–(d) H desorption rate for steel A and B after cathodic charging for 36 hrs, varying NH_4SCN concentration.

Fig. *7* shows a summary of the trends that were observed for the charging time and the influence of the inhibitor on the two steels in relation to the diffusible hydrogen content.

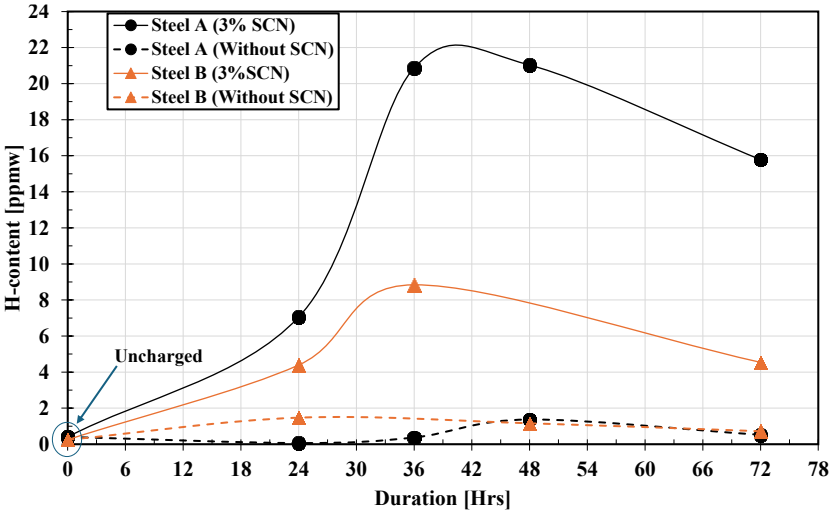

Fig. 7. A comparison of the hydrogen content for both steels after cathodic charging with 3%NH_4SCN and without.

3.3.2 Gaseous exposure

TDMS results obtained after hydrogen exposure at 260°C, 100 bars for a duration of seven days indicate hydrogen content of 0.01 ppm and 0.31 ppm for steel A and B respectively. The low hydrogen content levels obtained from gaseous exposure can be attributed to the probable loss of diffusible hydrogen during sample transfer from the autoclave to the TDMS analyser which took 48 hours due to experimental difficulties. To ensure more meaningful results, more tests still must be conducted.

4 Conclusions

- TDMS confirmed that hydrogen uptake was at a maximum for the charging duration between 36 and 48 hours for both steels.
- TDMS results obtained with the NH_4SCN addition proved the effectiveness of a hydrogen recombination inhibitor to enhance hydrogen uptake in steels during H–cathodic charging.
- The permeation transients acquired, as well as the diffusible H results, showed greater capacity of H uptake of steel A.

References

1. “Home | Green Hydrogen Organisation.” Accessed: Mar. 14, 2025. [Online]. Available: https://gh2.org
2. “South African Green Hydrogen Summit.” Accessed: Mar. 14, 2025. [Online]. Available: https://greenhydrogensummit.org.za
3. H. Zhang, J. Zhao, J. Li, B. Yu, J. Wang, R. Lyu, Q. Xi., Research progress on corrosion and hydrogen embrittlement in hydrogen–natural gas pipeline transportation, Nat. Gas. Ind. B, **10**, (2023).
4. X. Y. Cheng, H. Li, and X. B. Cheng, Carbides and possible hydrogen irreversible trapping sites in ultrahigh strength round steel, Micron, **103**, pp. 22–28, (2017), doi: 10.1016/j.micron.2017.09.005.

5. N. Yazdipour, A. J. Haq, K. Muzaka, and E. V. Pereloma, 2D modelling of the effect of grain size on hydrogen diffusion in X70 steel, Compu. Mater. Sci., **56**, pp. 49–57, (2012), doi: 10.1016/j.commatsci.2012.01.003.
6. R. Zhang, S. Ai, M. Long, L. Wan, Y. Li, D. Jia, H. Duan and D. Chen, Quantitative Study on Hydrogen Concentration–Hydrogen Embrittlement Sensitivity of X80 Pipeline Steel Based on Hydrogen Permeation Kinetics, Metals (Basel), **14**, no. 7, (2024), doi: 10.3390/met14070763.
7. S. Zheng, Y. Qin, W. Li, F. Huang, Y. Qiang, S. Yang, L. Wen, and Y. Jin, Effect of hydrogen traps on hydrogen permeation in X80 pipeline steel – a joint experimental and modelling study, Int. J Hydrogen Energy, **48**, no. 12, pp. 4773–4788, (2023), doi: 10.1016/j.ijhydene.2022.10.038.
8. F. Lang, F. Huang, J. Yue, L. Li, J. Xu, and J. Liu, Hydrogen trapping and hydrogen embrittlement (HE) susceptibility of X70 grade high-strength, acid-resistant, submarine pipeline steel with Mg treatment, J of Mat. Res. & Tech., **24**, pp. 623–638, (2023), doi: 10.1016/j.jmrt.2023.03.011.
9. D. Figueroa and M. J. Robinson, Hydrogen transport and embrittlement in 300 M and AerMet100 ultra high strength steels, Corro. Sci, **52**, no. 5, pp. 1593–1602, (2010), doi: 10.1016/j.corsci.2010.01.001.
10. J. Yong, N. A. Shamsuri, A. B. Bashir, M. F. Z. Kadir, and M. F. Abd Shukur, Effect of ammonium thiocyanate (NH4SCN) concentration on the ionic transport in dextran-based polymer electrolyte, Mol. Cry. and Liq. Cry., **764**, no. 1, pp. 55–69, (2023), doi: 10.1080/15421406.2023.2203561.
11. U. States, Standard Practice for Evaluation of Hydrogen Uptake, Permeation, and Transport in Metals by an Electrochemical Technique 1, **vol. i**, no. Reapproved, pp. 1–10, (2011), doi: 10.1520/G0148-97R11.2.
12. A. Metrohm, Corrosion Part 7 – Hydrogen permeation experiments with PGSTAT302F, Autolab Application Note COR07, pp. 2–3, [Online]. Available: Autolab_Application_Note_COR07.pdf.
13. A. Del-Pozo, J. C. Villalobos, and S. Serna, A general overview of hydrogen embrittlement, Curr. Tren. & Fut. Dev. (Bio-) Mem.: Adv. in Met. Mem., (2020), doi: 10.1016/B978-0-12-818332-8.00006-5.
14. M. N. Nazarova, R. R. Akhmetov, and S. A. Krainov, Temperature factors effect on occurrence of stress corrosion cracking of main gas pipeline, in IOP Conf. Ser.: Earth and Env. Sci., (2017). doi: 10.1088/1755-1315/87/6/062011.
15. X. Xu, R. Zhang, C. Wang, C. Liu, J. Zhang, and Y. Li, Experimental study on the temperature dependence of gaseous hydrogen permeation and hydrogen embrittlement susceptibility of X52 pipeline steel, Eng. Fail. Anal., **155**, (2023), doi: 10.1016/j.engfailanal.2023.107746.
16. J. Villalobos, A. Del-Pozo, B. Campillo, J. Mayen, and S. Serna, Microalloyed Steels through History until 2018: Review of Chemical Composition, Processing and Hydrogen Service, Metals (Basel), **8**, no. 5, p. 351, (2018), doi: 10.3390/met8050351.
17. R. D. K. Misra, H. Nathani, J. E. Hartmann, and F. Siciliano, Microstructural evolution in a new 770 MPa hot rolled Nb-Ti microalloyed steel, Mat. Sci. and Eng. A, **394**, no. 1–2, pp. 339–352, (2005), doi: 10.1016/j.msea.2004.11.041.
18. S. Zajac, Precipitation of microalloy carbo-nitrides prior, during and after γ/α transformation, Mat. Sci. For., **500–501**, pp. 75–86, (2005), doi: 10.4028/www.scientific.net/msf.500-501.75.
19. M. Ichiba, K. Takai, and J. Sakai, Effects of Test Conditions on Corrosion Reactions and Hydrogen Absorption in Hydrogen Embrittlement Tests Using an Ammonium Thiocyanate Solution, ISIJ Inter., **56**, no. 3, pp. 397–404, (2016), doi: 10.2355/isijinternational.ISIJINT-2015-288.

20. M. Ichiba, J. Sakai, T. Doshida, and K. Takai, Corrosion reaction and hydrogen absorption of steel for prestressed concrete in a 20mass% ammonium thiocyanate solution, Scr. Mater., **102**, pp. 59–62, (2015), doi: 10.1016/j.scriptamat.2015.02.013.
21. G. M. Pressouyre, A classification of hydrogen traps in steel, Met. Trans. A, **10**, no. 10, pp. 1571–1573, (1979), doi: 10.1007/BF02812023.
22. X. Li, J. Zhang, Y. Wang, B. Li, P. Zhang, and X. Song, Effect of cathodic hydrogen-charging current density on mechanical properties of prestrained high strength steels, Mat. Sci. and Eng.: A, vol. **641**, pp. 45–53, Aug. (2015), doi: 10.1016/j.msea.2015.06.003.